# Theoretical modelling on the deformation behaviour of auxetic tubular braid made from modified circular braiding technique

Ning Jiang, Yu Chen and Hong Hu*

Institute of Textiles and Clothing, The Hong Kong Polytechnic University, Hung Hom, Hong Kong, People Republic of China

*The corresponding author: hu.hong@polyu.edu.hk (Hong Hu)

**Abstract** This paper presents a theoretical analysis of auxetic tubular braid (ATB) formed with three types of component yarns having different diameter and modulus. A simple theoretical model is developed for predicting the deformation behaviour of this structure under uniaxial extension. With its accuracy firstly validated by the experimental data, the developed model is further corrected based on the real condition and thus becomes capable to characterize the auxetic behaviour of the ATB. During the analysis, it was found that the stiff wrap yarn cannot be fully straightened in real condition and its helical angle decreasing rate is inconsistent during the stretching. The present work, which provides an effective tool for understanding the deformation behaviour, is meaningful for the braid's improved design and applications.

**Keywords** Auxetic tubular braid, Deformation behaviour, Theoretical modelling, Geometrical analysis

**Nomenclature**

| | | | |
|---|---|---|---|
| $\nu$ | Poisson's ratio of ATB | $H$ | Effective diameter of ATB |
| $\nu_c$ | Poisson's ratio of core yarn | $D_c$ | Diameter of core yarn |
| $\nu_b$ | Poisson's ratio of braiding yarn | $D_b$ | Diameter of braiding yarn |

| | | | |
|---|---|---|---|
| $\nu_w$ | Poisson's ratio of stiff wrap yarn | $B_{mj1}$ | Major axis of braiding yarn at position 1 when stretched |
| $\varepsilon_l$ | Longitudinal tensile strain of ATB | $B_{mn1}$ | Minor axis of braiding yarn at position 1 when stretched |
| $\varepsilon_t$ | Lateral contractile strain of ATB | $B_{mj2}$ | Major axis of braiding yarn at position 2 when stretched |
| $\varepsilon_{cri}$ | Longitudinal tensile strain of ATB at the end of first stage | $B_{mn2}$ | Minor axis of braiding yarn at position 2 when stretched |
| $\varepsilon_c$ | Longitudinal tensile strain of core yarn | $D_w$ | Diameter of stiff wrap yarn |
| $\varepsilon_b$ | Longitudinal tensile strain of braiding yarn | $R$ | Helical radius of core yarn |
| $\varepsilon_w$ | Longitudinal tensile strain of stiff wrap yarn | $r$ | Helical radius of stiff wrap yarn |
| $p$ | Length of braiding yarn between two interlacement points | $L_c$ | Actual length of core yarn |
| $m$ | Distance between two interlacement points along the longitudinal direction | $L_b$ | Actual length of braiding yarn |
| $n$ | Distance between two interlacement points along the lateral direction | $L_w$ | Actual length of stiff wrap yarn |
| $L_{arcA}$ | Unit length of Arc A | $S_w$ | Helical length of stiff wrap yarn |
| $L_{arcB}$ | Unit length of Arc B | $\lambda_w$ | Cyclic pitch of the stiff wrap yarn |
| $\alpha$ | Helical angle of core yarn | $\lambda$ | Cyclic pitch of the ATB structure |
| $\theta$ | Helical angle of stiff wrap yarn | Subscript 0 | Indication of the initial state |
| $N$ | The number of braiding yarns of ATB | | |

## 1. Introduction

Auxetics refers to the materials and structures that display negative Poisson's ratio (NPR) [1]. Different from the common materials which tend to be thinner when stretched, auxetics will expand in the lateral direction upon stretching. This counterintuitive behaviour endows auxetics with a series of interesting properties, such as increased shear stiffness [2], enhanced

energy absorption [3], improved acoustic behaviour [4] and superior indentation resistance [4, 5], compared to conventional positive Poisson's ratio materials. Although the auxetics have been admitted to exist more than 100 years, a worldwide upsurge of research on these materials/structures only started from 1980s. Using Monte Carlo method, Wojciechowski and the co-author reported the occurrence of NPR in a two-dimensional system of hard cyclic hexamers [6, 7]. In 1987, Lakes [8] firstly fabricated a polyurethane foam with an obvious Poisson's ratio value, which made people realize that the auxetics could be obtained in a manmade way. Since then, tremendous numbers of auxetics have been developed, fabricated and synthesised [9-16], including the honeycombs, foams, composites and other special types, examples being the double helical yarn [17], folded fabric [18] and wine-rack structure [19].

In textile area, one of the most successful auxetic structures is the helical auxetic yarn (HAY) developed by Hook et al. in 2003 [17]. As shown in Figure 1, a HAY is constructed by a straight elastomeric core with a stiffer fibre helically wound around it. Upon tension, the stiff fibre which is in a helical form in the initial state would straighten and displace the core into a wave form. This shape deformation could then result in an expansion of HAY in the lateral direction if the diameter of the stiffer fibre is smaller than that of the elastomeric core [20]. According to the previous studies [21-23], the lateral shape deformation of HAY can lead to a maximum NPR over -10.0 when certain design configuration is selected. Based on theoretical analyses on HAY, four structural and material parameters, including the initial wrap angle of the stiff yarn, the Poisson's ratio of the core yarn and stiff yarn, relative modulus and diameter between the core yarn and stiff yarn, are found to have influence on auxetic behaviour of HAY. Especially, the initial wrap angle has the most important effect on auxetic behaviour of HAY. It is believed that a lower initial wrap angle can lead to a larger maximum NPR [20, 21, 24-26]. On the other hand, there may also exist an critical angle for obtaining the largest NPR, below or above which the maximum NPR of HAY will be

impeded [22]. With respect to the Poisson's ratio of core and stiff yarns, it is found that the auxetic effect of HAY is increased with the decrease in their Poisson's ratio [24]. This is mainly because the decrease in Poisson's ratio of component yarns can reduce the decrease in diameter of the component yarns when stretched, thus magnifying the lateral expansion effect (auxetic effect) of HAY. Meanwhile, an increase of the core/wrap diameter ratio can also enhance auxetic behaviour of HAY [22]. However, an elevated difference in component moduli would cause the wrap fibre embedding itself into the core fibre and thus reducing the auxetic effect of the whole HAY structure [23]. Therefore, careful determination of an optimum core/wrap moduli ratio where the ratio is high enough to yield an auxetic effect and low enough to prevent the core-indentation effect is critical in the real production of HAY.

Although the HAY can achieve high auxetic behaviour, it is also found that it has its own structural limitations. One of them is the slippage of the stiff yarn on the surface of the core yarn under repeated extension [20]. As the uniform wrapping of stiff yarn is the main driving force leading to the auxetic behaviour, this slippage effect could impair the performance of HAY when used in practical applications [27, 28]. In order to overcome this shortcoming, a new type of auxetic yarn called auxetic tubular braid (ATB) was recently proposed by the authors [29]. In the newly proposed structure, a third component yarn namely braiding yarn is added. The incorporation of the braiding yarn forms a braided sheath between the stiff wrap yarn and the elastic core yarn so that stiff wrap yarn can be fixed without using glue. Since this fixation occurs at evenly distributed points in each repeating turn, the stiff yarn can be wrapped onto the core uniformly in the new structure design. Up to the present, auxetic behavior of the ATB has been experimentally studied [29] but no theoretical analysis has been conducted on ATB yet, making its deformation mechanism unclear. As a new braiding layer is added into the ATB, the geometrical models previously developed for the HAY [25, 26] are no longer suitable for calculating the Poisson's ratio of

the ATB even though both two structures have a similar deformation behaviour under tension. In this regard, a theoretical analysis focused on deformation mechanism of ATB is conducted and presented in this paper in order to better understand this new structure. The new model is developed based on a geometrical analysis of the ATB structure and experimental work so that its Poisson's ratio under uniaxial extension condition can be predicted.


Figure 1. HAY structure at zero strain [17].

## 2. Geometry and deformation

Figure 2a shows one complete cycle of the ATB structure. It can be seen that the stiff yarn in ATB structure is helically wrapped onto the core yarn and fixed by other numerous braiding yarns. Compare to the perfect helical shape of stiff wrap yarn in HAY structure, the shape of the stiff wrap yarn in ATB structure at zero strain is irregular because of the interlacement effect at fixing points. As a result, different deformation mechanism is presented in ATB structure compared to HAY under tension. In this study, we divide the overall shape deformation of the ATB structure into two stages (Figure 2b) and describe them as follows.

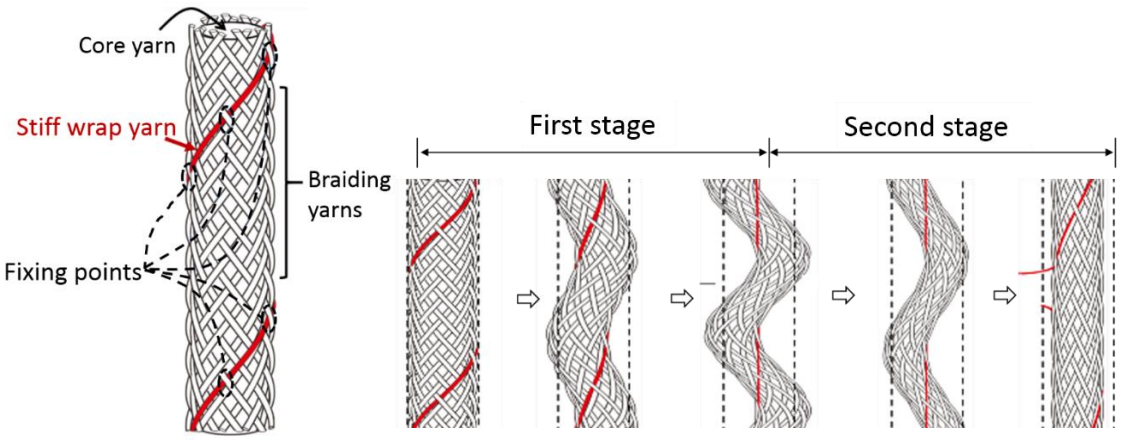

(a) (b)

Figure 2. ATB structure: (a) geometry at zero strain and (b) the shape deformation under tension.

### 2.1 First stage

The first stage starts from the initial state and ends when the stiff wrap yarn becomes straight along the longitudinal axis of ATB structure. In this stage, the stiff wrap yarn changes from an irregular shape to a helical shape and finally become a straight line with the increase of tensile strain. During the same time, the shape of the base braid formed by the core yarn and braiding yarns changes from a straight line to a helical shape. This helical shape deformation of the base braid would result in an expansion of the whole structure in lateral direction as the braid has a larger diameter than the stiff yarn. Regarding the Poisson's ratio value of ATB structure, it is positive firstly due to the cross-sectional contraction of three component yarns and then decrease to a negative value because of the helical shape deformation of the base braid.

### 2.2 Second stage

The second stage starts from the end of the first stage and finishes when the stiff wrap yarn breaks. In this stage, the stiff wrap yarn has become straight along the longitudinal axis of ATB structure and thus its helical radius is equal to zero. Further stretching would cause the stiff wrap yarn to have length elongation along the longitudinal axis of ATB structure. Meanwhile, the base braid is still in a helical shape but its helical radius starts to decrease with the increase of tensile strain because the stiff wrap yarn cannot displace the base braid laterally heretofore. Regarding the Poisson's ratio of ATB structure, its negative value starts to decrease because there is no further lateral expansion of the whole structure and yet the cross section of component yarns continually decreases with the increase of the tensile strain.

### 2.3. Basic assumptions

To facilitate the theoretical analysis on the structure deformation in above two stages, the following assumptions are made first. All symbols used during the analysis can be found in Nomenclature for easy check and reference.

(1) The Poisson's ratio of all component yarns is constant during the whole tensile process.

(2) The cross-section shape of stiff wrap yarn and core yarn is circular in the initial state and keeps circular when stretched. This is because the stiff wrap yarn is difficult to be compressed under low loading while the core yarn receives an even pressure from the braiding yarns that circularly covers it.

(3) The cross-section shape of braiding yarns is circular in the initial state but becomes ellipse when stretched. This is because the braiding yarns are easy to be compressed under low loading. Based on the experimental results, we assume the cross-section of the braiding yarns which are placed under the stiff wrap yarn is an ellipse with a fixed minor axis/major axis ratio of 0.81, while the cross-section of the braiding yarns which are placed under other braiding yarns are ellipses with a fixed minor axis/major axis ratio of 0.95 during the whole stretching process. The minor axis/major axis ratios of the two ellipses are assumed to have fixed values in order to simplify the analysis.

(4) The fixing points of the stiff wrap yarn have fixed positions relative to the whole structure due to the large mutual constraint at fixing points. At the same time, it is assumed that all three component yarns are contacted closely to each other from the initial state to the failure of the stiff wrap yarn.

(5) The deformation process of ATB can be divided into two stages as mentioned above. In the first stage, the length and the cross-section area of the stiff wrap yarn are assumed to be constant because the stiff wrap yarn are difficult to be extended under a low loading

condition and increased tensile strain will only reduce its helix radius. However, in the second stage, the cross-section area and length of the stiff wrap yarn are no longer constant because its higher tensile strain.

(6) It is assumed that the straightening rate of the stiff wrap yarn is constant in the first stage because the whole analysis conducted here is based on a constant-rate extension condition.

## 3. Analytical modelling

### 3.1. Initial state

Figure 3a and 3b respectively schematically shows the geometry of the ATB structure and its cross section in the initial state. As the major reason for the lateral expansion of the ATB structure is the helical shape change during the stretching, we would like to start the analysis from the helical radius of the core yarn and the helical radius of stiff wrap yarn. The helical radius of the braiding yarns is not analysed here because the braiding yarns can be regarded as part of the core yarn, i.e., they share a same helical radius.

Let us start with the initial helical radius of core yarn, $R_0$. As shown in Figure 3a, the core yarn is a straight line in the initial state and its longitudinal axis is coincident with the longitudinal axis of the ATB structure. Therefore, we have $R_0$ in Eq. (1),

$$R_0 = 0 . \tag{1}$$

Regarding the initial helical radius of stiff yarn, $r_0$, it can be given by Eq. (2) based on the Figure 3b and the assumption that all three component yarns have a circular shape in the initial state.

$$r_0 = \frac{D_{c0} + 2D_{b0} + D_{w0}}{2} . \tag{2}$$

With the above two helical radii, the effective diameter of ATB in the initial state, i.e., $H_0$, can be obtained as:

$$H_0 = \begin{cases} 2r_0 + D_{w0}, & (D_{w0} > D_{b0}), \\ 2R_0 + D_{c0} + 4D_{b0}, & (D_{w0} < D_{b0}). \end{cases} \tag{3}$$

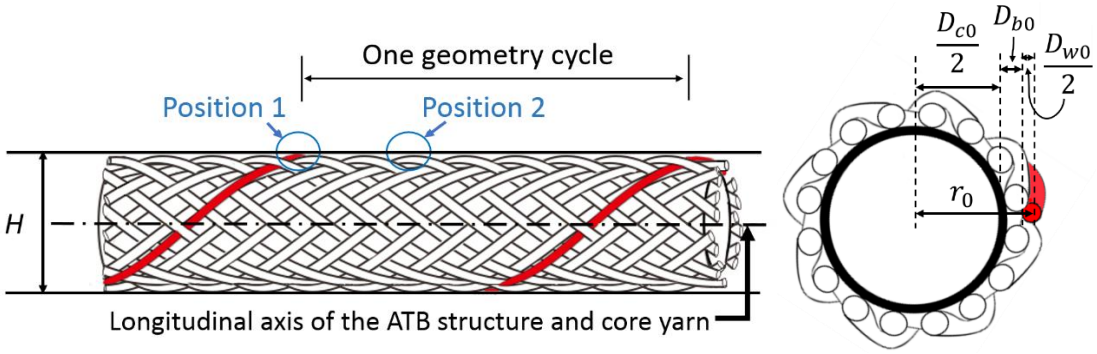


(a) (b)

Figure 3. ATB structure in the initial state: (a) one complete geometry cycle and (b) cross section.

Eq. (3) indicates that $H_0$ needs to be determined differently according to the different diameter ratio between the stiff yarn and braiding yarns. When $D_{w0} > D_{b0}$, $H_0$ is obtained from interlacing points between the stiff wrap yarn and the braiding yarn, i.e., Position 1 in Figure 3a; when $D_{w0} < D_{b0}$, $H_0$ is obtained from the interlacing points between two braiding yarns, i.e., Position 2 in Figure 3a; when $D_{w0} = D_{b0}$, $H_0$ obtained from those two positions are same.

Apart from the above, there is another critical parameter existing in the initial state and it is the initial actual length of the stiff wrap yarn, $L_{w0}$. As shown in Figure 4, $L_{w0}$ is different from $S_{w0}$ ($S_{w0}$ is the perfect helical length of stiff wrap yarn at the initial state) because the path of stiff wrap yarn in ATB is not a perfect helix in the initial state. This difference between $L_{w0}$ and $S_{w0}$ could influence the straightening of the stiff wrap yarn and thus have an

effect on the deformation behaviour of ATB structure under tension. Therefore, a clear clarification and expression for $L_{w0}$ and $S_{w0}$ are required in our analytical model.

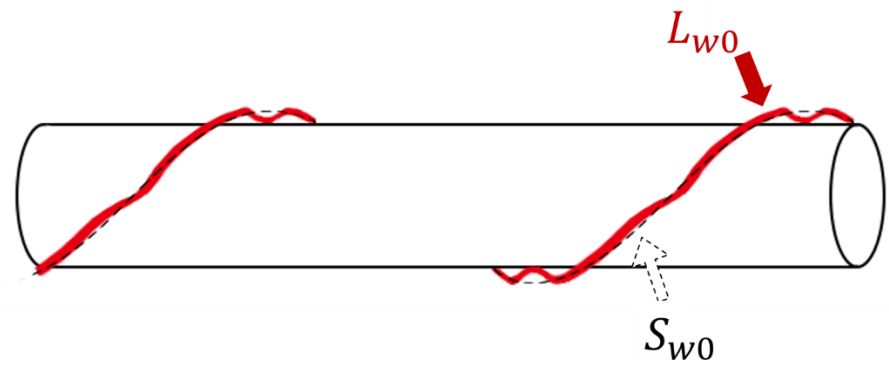


Figure 4. The path of stiff wrap yarn along the ATB surface in the initial state (indicated by the red line).

First, we would like to determine the geometry shape of $L_{w0}$. As shown in Figure 5a, the irregular shape of stiff yarn can be regarded as a curve formed by two types of arcs: Arc A and Arc B. As shown in Figure 5b, Arc A is resulted from interlacing the stiff yarn with other braiding yarns while Arc B is resulted from wrapping the stiff yarn helically onto the ATB structure.

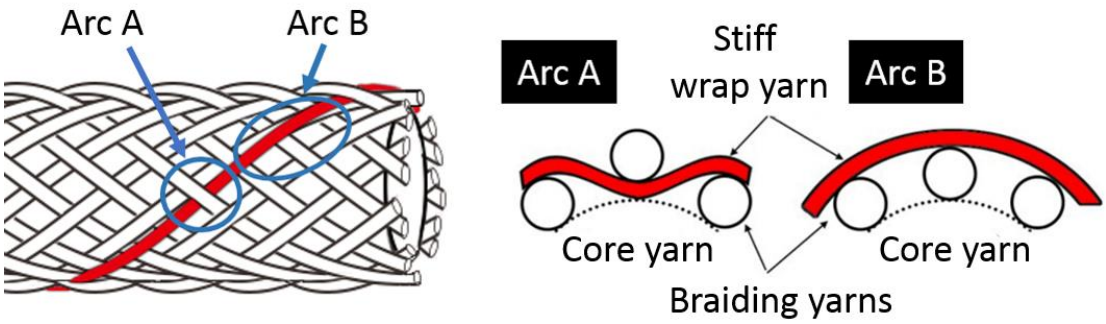


(a) (b)

Figure 5. Two types of arcs which form irregular path of the stiff wrap yarn in the initial state: (a) see from front-view and (b) see from side-view.

Since there exist certain geometry relationships in these two types of arcs, the length of stiff wrap yarn can be calculated. As shown in Figure 6a. Arc A is similar to the shape of warp yarns formed in a woven fabric and thus its unit length, $L_{arcA}$, can be determined by using Peirce's approximate formula for woven threads as:

$$L_{arcA} = \frac{64\pi^2 r_0 + 9N^2 {D_{b0}}^2}{32N\pi r_0} \quad . \tag{4}$$

Meanwhile, Arc B can be regarded as a part of circle of which the radius is $r_0$, as shown in Figure 6b. Therefore, its unit length, $L_{arcB}$, can be solved and is given by Eq. (5):

$$L_{arcB} = \frac{2\pi r_0}{N} . \tag{5}$$

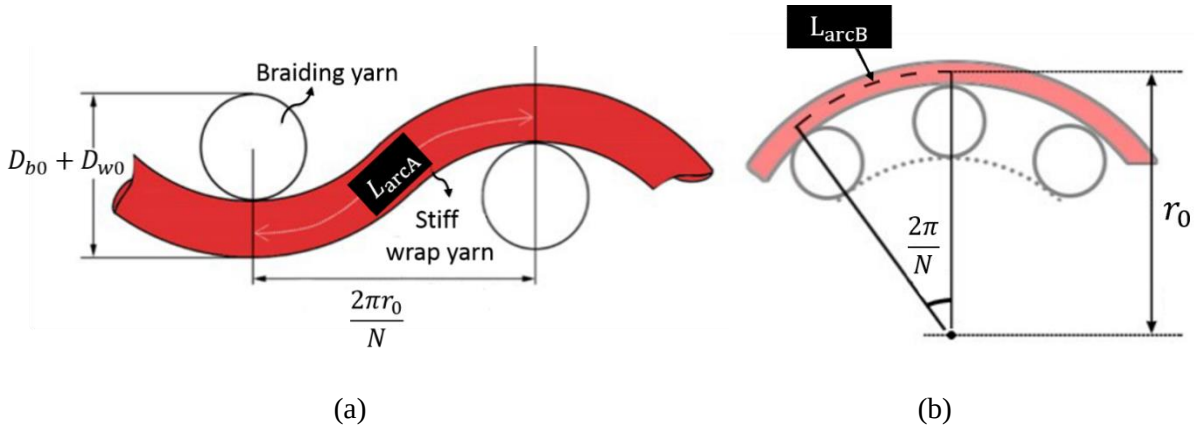


(a) (b)

Figure 6. The geometry relationships existed in (a) Arc A and (b) Arc B.

Since the unit length of the two arcs corresponds to dimension that is perpendicular to the longitudinal axis of ATB, $L_{w0}$ is equal to the sum of $L_{arcA}$ and $L_{arcB}$ divided by $\sin\theta_0$. In case of our ATB structure where an interlacement between the stiff wrap yarn and other braiding yarns occurs at every 90°, there are $8L_{arcA}$ and $(N-8)L_{arcB}$ in one complete ATB geometry cycle. Therefore:

$$L_{w0} = \frac{8L_{arcA} + (N-8)L_{arcB}}{\sin\theta_0} = \frac{8\pi^2 r_0^{\,2} + 9ND_{b0}^{\,2}}{4\pi r_0 \sin\theta_0} \quad . \tag{6}$$

Now in order to determine the parameter, $S_{w0}$, we use the triangular relation existing in the helical length of the stiff wrap yarn and its helical radius. Based on the relationship shown in Figure 7a, $S_{w0}$ and together the cyclic pitch of the stiff wrap yarn, $\lambda_{w0}$, is given by Eq. (7) and Eq. (8), respectively:

$$S_{w0} = \frac{2\pi r_0}{\sin\theta_0} \quad , \tag{7}$$

and

$$\lambda_{w0} = \frac{2\pi r_0}{\tan\theta_0} \, . \tag{8}$$

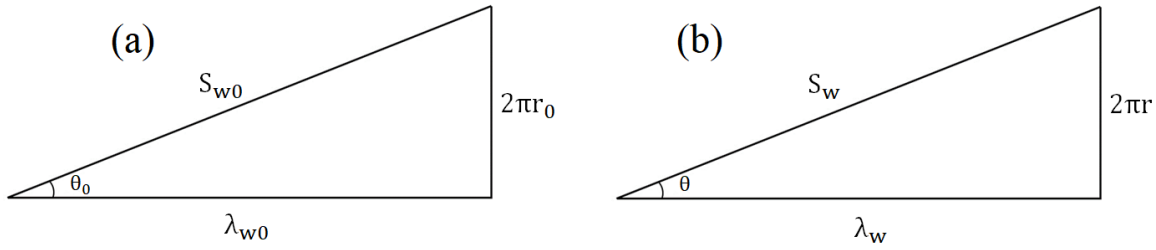


Figure 7. The triangular relationship between the helical length and helical radius of the stiff wrap yarn (a) the initial state; (b) the first stage (Section 3.2).

### 3.2. The first stage

Figure 8 shows the geometry of the ATB structure in the first stage. In this stage, the helical radii of stiff wrap yarn and core yarn, $r$ and $R$, are changing according to the tensile strain $\varepsilon_l$. Let us determine $r$ firstly.

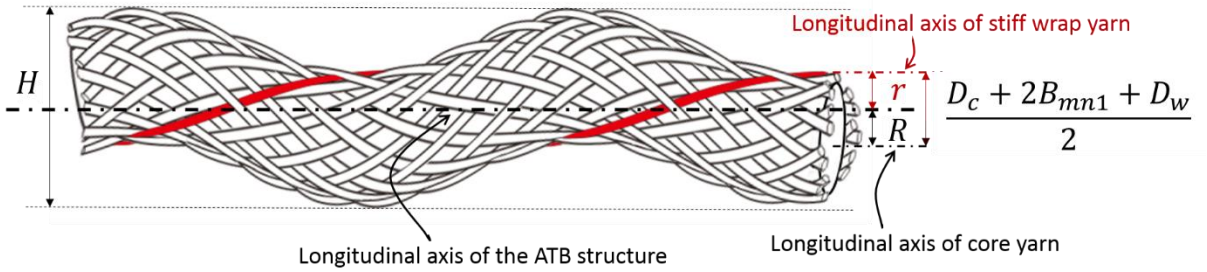


Figure 8. Geometry of the ATB structure in the first stage.

Similar to the initial state, there exists a triangular relation between the helical length $S_w$ and the helical radius of the stiff wrap yarn $r$ (Figure 7b). Based on that relationship, we have:

$$r = \frac{\sqrt{S_w^{\,2} - \lambda_w^{\,2}}}{2\pi}. \tag{9}$$

Eq. (10) indicates $S_w$ and $\lambda_w$ needs to be known in order to calculate $r$. Thus, we calculate $S_w$ firstly. As it can be seen from Figure 9, $S_w$ is not equal to $L_w$ until the stiff yarn becomes straight along the longitudinal axis of the ATB structure, i.e., the end of the first stage. Based on that, we have $S_w$ given in Eq. (10) with the assumption that the straightening rate of stiff wrap yarn is constant in the first stage:

$$S_w = \frac{L_w - S_0}{\left(L_w - \lambda_0\right)/\lambda_{w0}} \cdot \varepsilon_l + S_{w0}. \tag{10}$$

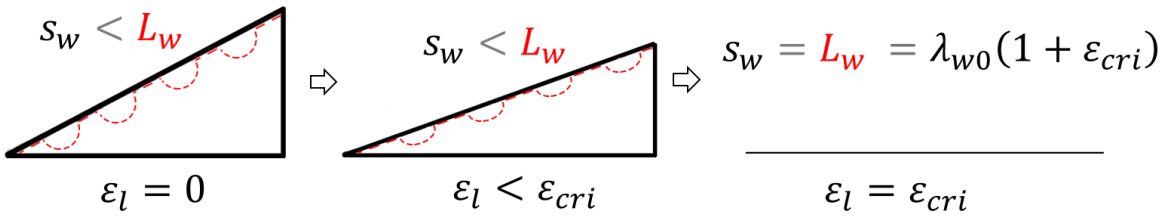


Figure 9. The relationship between $S_w$ and $L_w$ in the first stage ($\varepsilon_{cri}$ is the longitudinal tensile strain of ATB at the end of the first stage).

Meanwhile, $\lambda_w$ can be easily obtained by Eq. (11):

$$\lambda_w = \lambda_{w0}\left(1+\varepsilon_l\right). \tag{11}$$

As it is assumed that stiff wrap yarn has no longitudinal elongation in the first stage, $L_w$ is equal to $L_{w0}$. Thus, we finally have $r$ by substituting Eqs. (7), (8), (10) and (11) into Eq. (9):

$$r = r_0\sqrt{\left(\frac{18ND_{b0}{}^2}{\tan\theta_0+18ND_{b0}{}^2\tan\theta_0-\sin\theta_0}\varepsilon_l+\frac{1}{\sin\theta_0}\right)^2-\frac{\left(1+\varepsilon_l\right)^2}{\tan^2\theta_0}}. \tag{12}$$

Regarding $R$, it is calculated based on the geometry relations in Figure 8 by Eq. (13):

$$R = \frac{\left(D_c+2B_{mn1}+D_w\right)}{2}-r, \tag{13}$$

where $B_{mn1}$ (the minor axis of braiding yarn at Position 1) is used because the cross section of braiding yarn under the stiff yarn is in an ellipse shape under tension. From Eq. (13), it can be seen that $D_c$, $B_{mn1}$ and $D_w$ are three key parameters to determine $R$ and will be calculated in the following, respectively.

(i) Determination of $D_c$

Since the ATB structure and the core yarn are in a straight form in the initial state, it can be known that the initial actual length of the core yarn $L_c$ in a repeating cycle is equal to the initial cyclic pitch of the ATB structure $\lambda_0$. Based on that and the triangle relationship presented in Figure 10, the longitudinal tensile strain of the core yarn $\varepsilon_c$ at strain of the ABC $\varepsilon_l$ is derived as:

$$\varepsilon_c = \frac{\sqrt{\left(2\pi R\right)^2+\lambda^2}-\lambda_0}{\lambda_0}. \tag{14}$$

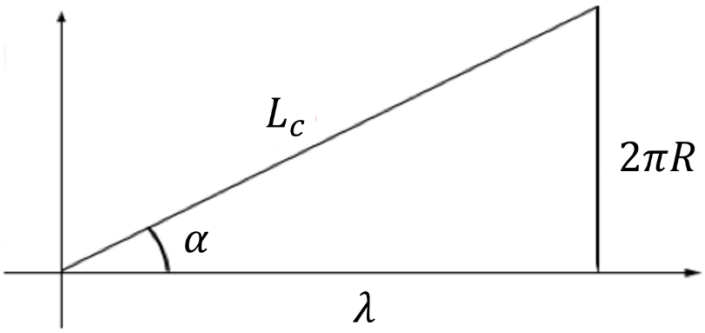


Figure 10. The triangle relationship exists in the path of core yarn.

Meanwhile, based on the assumption (4), it can be known that $\lambda_0 = \lambda_{w0}$ and further $\lambda = \lambda_w$. Therefore, with Eqs. (11) and (14), we have,

$$\varepsilon_c = \frac{\sqrt{(2\pi R)^2 + \lambda_{w0}{}^2 (1+\varepsilon_l)^2}}{\lambda_{w0}} - 1. \tag{15}$$

Based on the Poisson's law, $D_c$ can be described by

$$D_c = D_{c0}(1 - \nu_c \varepsilon_c). \tag{16}$$

(ii) Determination of $B_{mn1}$

In order to calculate $B_{mn1}$, it is necessary to know the longitudinal tensile strain of braiding yarns, $\varepsilon_b$. Under that circumstance, one interlacement unit between two braiding yarns is illustrated and presented in Figure 11. Using Peirce's approximate formula for woven threads, the actual length of the braiding yarn $L_b$ is:

$$L_b = 8\left\{(B_{mj2} - B_{mn2}) + \left[p - (B_{mj2} - B_{mn2})\right]\left[1 + \frac{(3B_{mn2})^2}{(4p)^2}\right]\right\}. \tag{17}$$

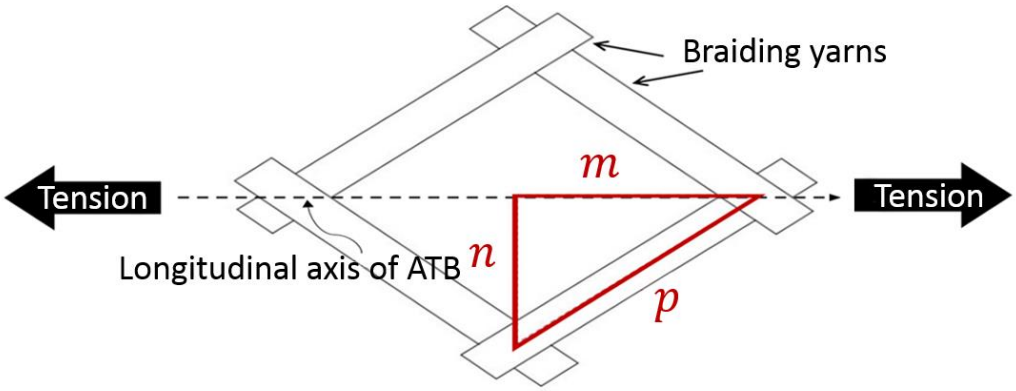


Figure 11. The interlacement unit between two braiding yarns in ATB structure.

Noted here $B_{mj2}$ and $B_{mn2}$ are used instead of $B_{mj1}$ and $B_{mn1}$ because braiding yarns have a same longitudinal tensile strain at both Position 1 and Position 2 and it is easy to calculate from Position 2. As $\left(B_{mj2}-B_{mn2}\right)$ and $\left(B_{mn2}\right)^2$ are much smaller than $p$, $\varepsilon_b$ is given below:

$$\varepsilon_b=\frac{L_b}{L_{b0}}-1=\frac{p}{p_0}-1, \tag{18}$$

where $p$ and $p_0$ is given as:

$$\begin{cases} p=\sqrt{m^2+n^2} \\ p_0=\sqrt{m_0{}^2+n_0{}^2} \end{cases}, \tag{19}$$

with

$$\begin{cases} m_0=\dfrac{\lambda_0}{N} \\ m=\left(1+\varepsilon_c\right)m_0 \end{cases}, \tag{20}$$

and

$$\begin{cases} n_0=\dfrac{2\pi D_{c0}}{N} \\ n=\dfrac{2\pi D_c}{N} \end{cases}. \tag{21}$$

As $\lambda_0 = \lambda_{w0}$ , we have $\varepsilon_b$ in Eq. (22) by substituting Eqs. (8), (14), (16) and (19) into Eq. (18):

$$\varepsilon_b = \frac{\sqrt{4R^2 \tan^2\theta_0 + 4{r_0}^2\left(1+\varepsilon_l\right)^2 + 4{D_{c0}}^2\left(1-\nu_c\varepsilon_c\right)^2 \tan^2\theta_0}}{\sqrt{4{r_0}^2 + 4{D_{c0}}^2 \tan^2\theta_0}} - 1, \tag{22}$$

According to the assumption (3) and Eq. (22), $B_{mn1}$ is given in Eq. (23) by Poisson's law:

$$B_{mn1} = \sqrt{0.81} D_{b0}\left(1-\nu_b\varepsilon_b\right). \tag{23}$$

(iii) Determination of $D_w$

As it is assumed that the cross-section of stiff wrap yarn is constant in the first stage. We have,

$$D_w = D_{w0}. \tag{24}$$

At this point, the relation between the helical radius of core yarn, $R$, and longitudinal strain, $\varepsilon_l$ , is built by substituting Eqs. (12), (16), (23) and (24) into Eq. (13). As the diameter of all component yarns and helical radius of stiff wrap yarn and core yarn are not constant in the first stage, the effective diameter of ATB structure, $H$, has also changed. Based on the similar relationship in Eq. (3), $H$ is described by Eq. (25):

$$H = \mathrm{Max}\begin{cases} 2r + D_w, \\ 2R + D_c + 4B_{mn2}. \end{cases} \tag{25}$$

with

$$B_{mn2} = \sqrt{0.95} D_{b0}\left(1-\nu_b\varepsilon_b\right). \tag{26}$$

Apparently, the effective diameter of ATB structure, *H*, can be expressed as a monodromic function of longitudinal strain, $\varepsilon_l$, according to above derivations.

### 3.3. The second stage

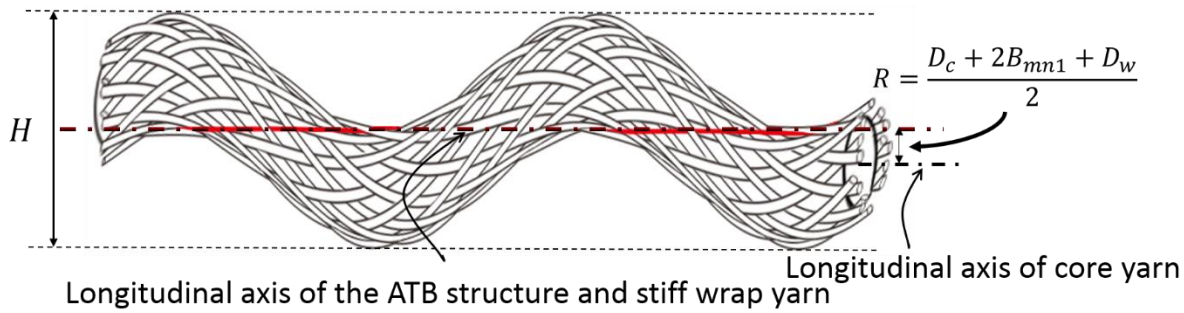


Figure 12. Geometry of the ATB structure in the second stage.

Figure 12 shows one complete geometry cycle of the ATB structure in the second stage. In the second stage, the value of $r$ becomes zero because the stiff wrap yarn gets straight along the longitudinal axis of the ATB structure. Therefore, only $R$ is needed to be determined in this stage. Based on the geometry relationship in Figure 12, $R$ is given as:

$$R = \frac{\left(D_c + 2B_{mn1} + D_w\right)}{2}. \tag{27}$$

As the changes in $D_c$, $B_{mn1}$ are continuous from the beginning of the first stage to the end of the second stage, the mathematical expressions for $D_c$ and $B_{mn1}$ presented in Eqs. (16) and (23) are still valid in the second stage. Meanwhile, $D_w$ needs to be determined independently because the cross section of stiff wrap yarn is no longer constant in the second stage.

Based on the assumptions that the stiff wrap yarn has no elongation in the first stage and becomes straight along the longitudinal axis of the structure at the end of first stage, it can be found that the actual length of stiff wrap yarn $L_w$ has the following relationship with $\varepsilon_l$ in the second stage:

$$L_w = \lambda_0\left(1+\varepsilon_l\right). \tag{28}$$

As $L_w = L_{w0}(1+\varepsilon_w)$ and $\lambda_0 = \lambda_{w0}$, we have the longitudinal tensile strain of the stiff wrap yarn, $\varepsilon_w$, based on the Eqs. (6), (8) and (28):

$$\varepsilon_w = \frac{8\pi(1+\varepsilon_l)r_0^{\,2}\cos\theta_0}{8\pi r_0^{\,2} + 9N{D_{b0}}^2} - 1. \tag{29}$$

Therefore, $D_w$ is calculated based on the Poisson's law:

$$D_w = D_{w0}(1-\nu_w\varepsilon_w). \tag{30}$$

As the value of *H* measured from Position 2 is always larger than that measured from the Position 1 in this stage, the effective diameter of ATB structure in the second stage can be given as:

$$H = 2R + D_c + 4B_{mn2}. \tag{31}$$

### 3.4. Critical strain, $\varepsilon_{cri}$ , between the two stages.

It is important to know the critical strain which separates the first stage and second stage, $\varepsilon_{cri}$. This can be determined by the fact that the stiff yarn has no elongation in the first stage and it becomes straight along the center line of the structure at the end of first stage as:

$$\varepsilon_{cri} = \frac{L_{w0}}{\lambda_{w0}} - 1. \tag{32}$$

By substituting Eqs. (6) and (8) into Eq. (32), the critical strain can be further calculated as:

$$\varepsilon_{cri} = \frac{8\pi^2 r_0^{\,2} + 9N{D_{b0}}^2}{8\pi^2 r_0^{\,2}\cos\theta_0} - 1. \tag{33}$$

### 3.5. Determination of Poisson's ratio

Based on the above, the Poisson's ratio of the ATB structure, $\nu$, as a function of the tensile strain, $\varepsilon_l$, can be finally obtained:

$$\nu = -\varepsilon_t \times \frac{1}{\varepsilon_l} = -\frac{H - H_0}{H_0} \times \frac{1}{\varepsilon_l}. \tag{34}$$

Eq. (34) indicates that the relationship between $\nu$ and $\varepsilon_l$ can be obtained once the effective diameter in the initial state $H_0$ and the effective diameter in the stretched state $H$ are known. With that in mind, Figure 13 shows the calculation process of $\nu$ in detail.

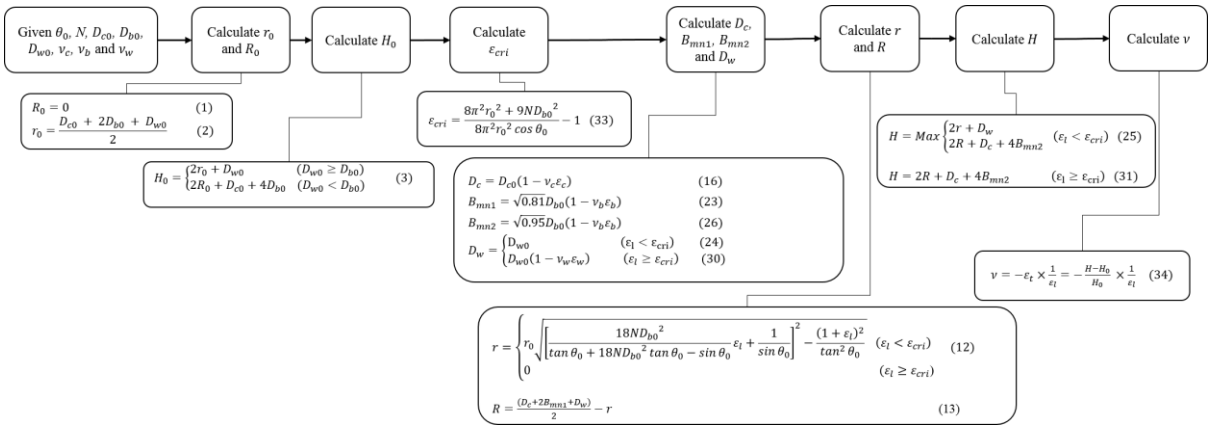


Figure 13. The calculation procedure for the Poisson's ratio of the ATB.

## 4. Experiment verification and model correction

The parameters measured on ATB samples and component yarns prior to testing are shown in Table 1. These initial parameters were used for the theoretical calculation of the Poisson's ratio of ATB structure under tension.

Table 1. The geometrical parameters in the initial state used for calculation.

| $\theta_0(°)$ | $N$ | $D_{c0}$ (mm) | $D_{b0}$ (mm) | $D_{w0}$ (mm) | $\nu_c$ | $\nu_b$ | $\nu_w$ |
|---|---|---|---|---|---|---|---|
| $32 \pm 1$ | 16 | 2.5 | 0.32 | 0.19 | 0.47 | 0.47 | 0.33 |

Tensile testing was performed on Instron 5944 tensile tester according to the ASTM D2653. The Poisson's ratio of samples was measured by counting the pixel between sample

boundaries. The experimental Poisson's ratio-strain curve used for the comparison (see Figure 14) is the average value of three sample results.

Figure 14 shows, respectively, the Poisson's ratio-strain curves that are calculated from theory and obtained from experiments. It can be seen that the trend of calculated curve is very close to the experimental one, especially when the tensile strain is smaller than 17%. This indicates the good agreement between the developed analytic model and real ATB structure deformation under tension. However, it can also be seen that there exists an evident difference between calculated curve and experimental one after the tensile strain exceeds 17%. We believe this difference is mainly resulted from the existence of diameter and modulus of core yarn and braiding yarn, which could resist the straightening of stiff wrap yarn. Because of that resistance effect, the helical wrap angle of stiff wrap yarn, $\theta$, cannot reach the zero value in real practice. As it is assumed that stiff wrap yarn can be fully straightened to a zero degree in our analytical model, the calculated maximum NPR value is significantly higher than experimental one.

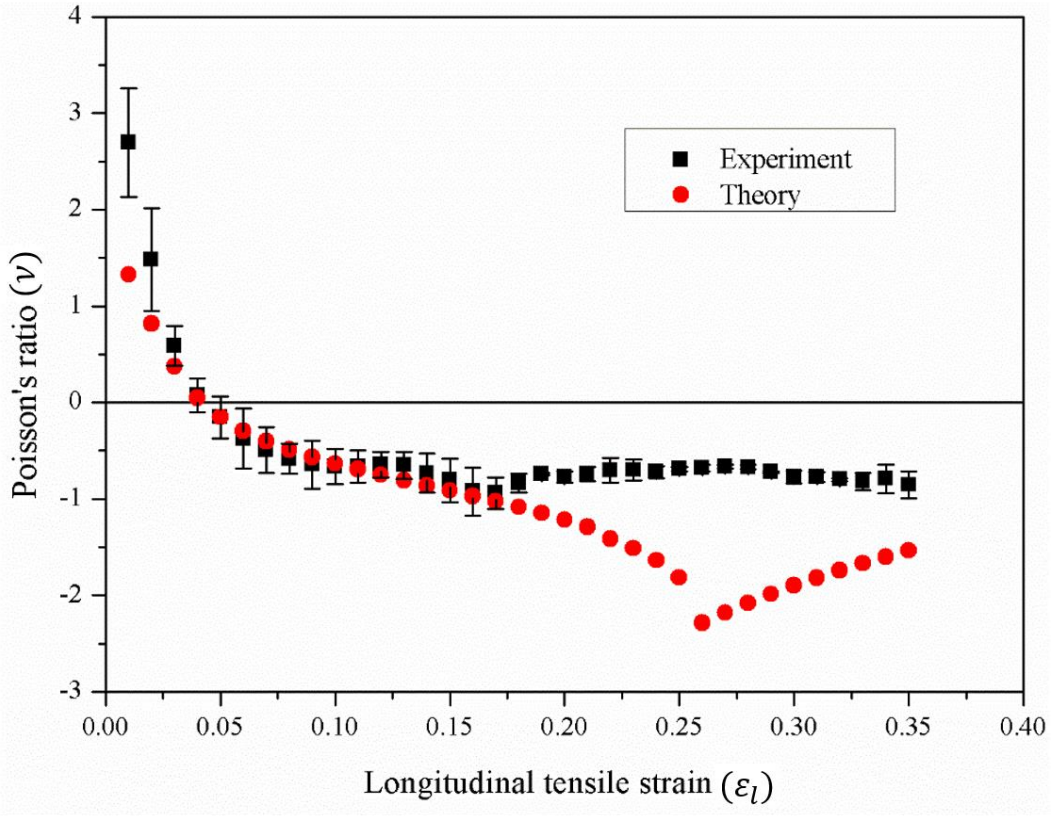


Figure 14. Comparison between Poisson's ratio of ATB structure calculated from theory and obtained from the experiment.

In order to confirm our hypothesis on the cause of difference between calculated results and experiment, the change of $\theta$ during tensile testing is analysed. As shown in Figure 15, it can be found that the value of $\theta$ is around $5.1°$ when the stiff wrap yarn eventually fails at a 35% strain during the tensile testing. This angle can be considered as critical angle. It indicates that the stiff wrap yarn in ATB structure cannot be fully straightened (at least under the condition of our used three component yarn). Based on that, the assumption in analytical model that stiff wrap yarn can be fully straightened to a zero degree is not very realistic and thus can result in the difference between calculated results and experiment at higher tensile strain. On the other hand, it can also be seen that the decrease rate of $\theta$ is not constant during the stretching. Before 17% tensile strain, $\theta$ is almost linearly decreasing with the increase of

the tensile strain. After 17% tensile strain, the decrease rate of $\theta$ is significantly reduced and there presents a second-degree polynomial relationship between $\theta$ and $\varepsilon_l$ after 17% tensile strain, as presented below：

$$\theta = 191.31\varepsilon_l^{\,2} - 132.69\varepsilon_l + 27.99\,. \tag{35}$$

This inconstant decrease rate of $\theta$ in real practice is also responsible for the huge difference between calculated results and experiment because $\theta$ in analytical model is sharply decreased to $0°$ after 17% tensile strain (Figure 15).

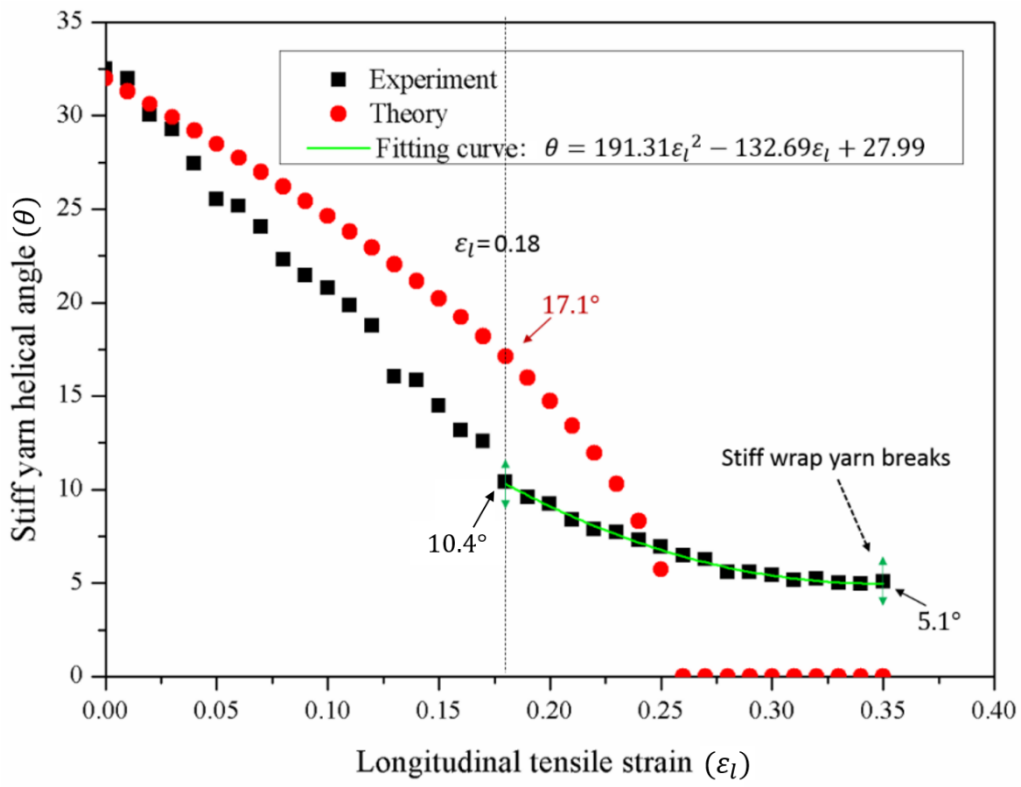


Figure 15. The relationship between $r$ and $\varepsilon_l$ calculated from theory and obtained from the experiment.

Under this circumstance, we believe it is necessary to adjust the analytical model with reference to the real condition. Therefore, we recall the stiff yarn can be fully straightened

and assume that $\theta$ in analytical model also has a second-degree polynomial relationship with $\varepsilon_l$ as presented below：

$$\theta = 191.3\varepsilon_l^{\,2} - 132.69\varepsilon_l + 27.99 + (17.1 - 10.4). \tag{36}$$

Noted here (17.1-10.4) is the value difference between calculated $\theta$ and experimental $\theta$ at the 18% tensile strain (see Figure 15). With Eq. (36) and Figure 9, the calculation of $r$ after 17% tensile strain now is given by Eq. (37) instead of Eq. (12).

$$r = \lambda_{w0}(1+\varepsilon_l)\tan\theta. \tag{37}$$

Figure 16 then presents the results from experiment, analytical model with and without modification. It can be seen that the difference between the calculated results and experiment is significantly reduced after modification. The relationship between $\theta$ and $\varepsilon_l$ which calculated from the modified theory is compared to that obtained from experiment, as shown in Figure 17, and a general good agreement is observed. Given above, the modified theoretical model can successfully characterize the deformation behavior of the new ATB structure.

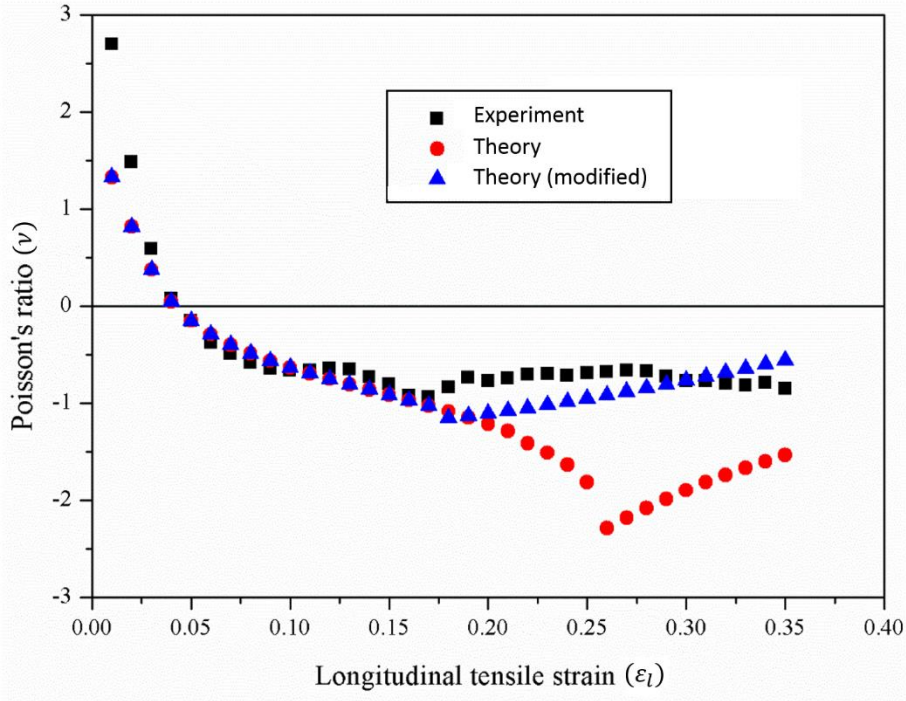

Figure 16. Comparison of Poisson's ratio of ATB structure obtained from the experiment and calculated from analytical model with and without modification.

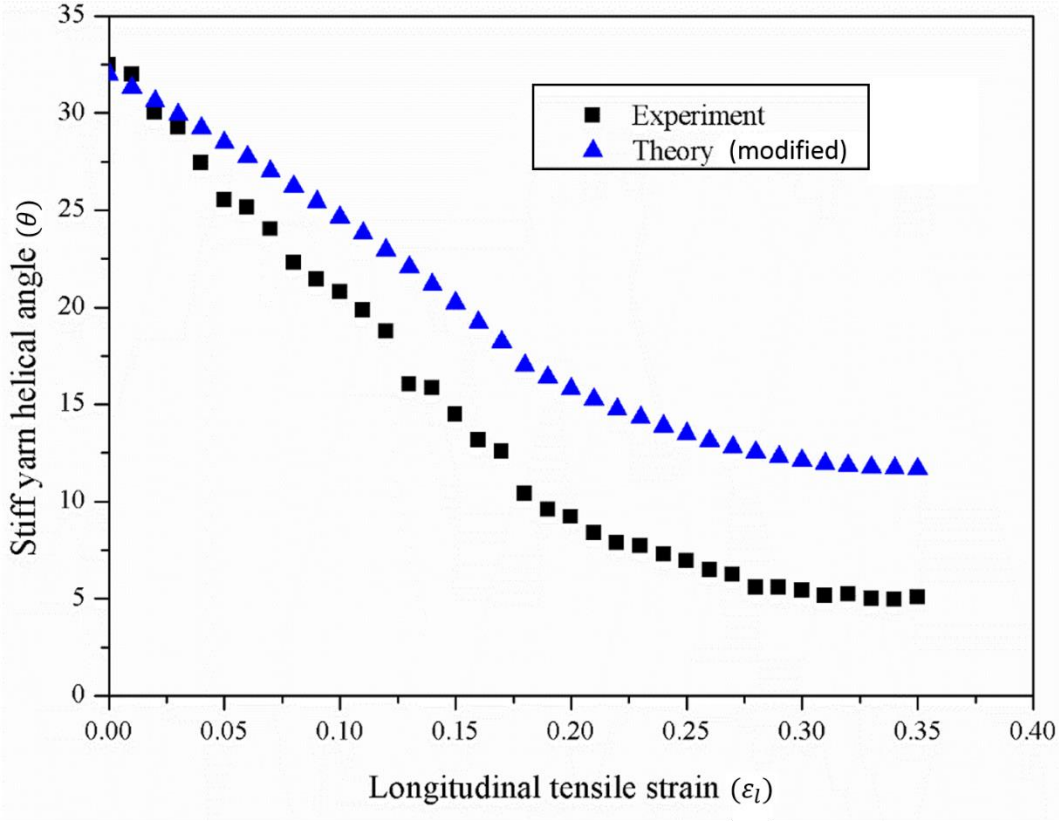


Figure 17. The relationship between $\theta$ and $\varepsilon_l$ calculated from modified analytical model and obtained from experiment.

As mentioned above, the analytical model is quite close to the experiment (Figure 16) before the critical strain point ($\varepsilon_l$=17%) but dramatically deviates from the experiment after $\varepsilon_l$=17%. The reason for the difference in the interval of $\varepsilon_l > 17\%$ lies in the assumption adopted during the analytical analysis (the stiff yarn is fully straightened) does not match with reality. Obviously, the analytical model is of acceptable accuracy for any structure with given material and geometric parameters before the critical strain point. While for the case of $\varepsilon_l > 17\%$, we presented an adjustment on the analytical model to make it more comprehensive. This adjustment is conducted based on the fitting of experimental data (see Eq.(36)). As a result, the adjustment is related to the choice of ATB materials and geometry, which means that different ATB materials and geometry will result in different polynomial coefficients in Eq.(36). However, the theoretical model does not lose its scientific value and it

can still be used as a guideline for structure design and the prediction of the deformation behaviour of ATB made with the same materials. As shown in Fig.18, effect of the initial wrap angle of the stiff yarn on the Poisson's ratio could be predicted using the developed model. It should be noted that ATB structures with different levels of the initial wrap angle are expected to fail at the same critical angle value because the critical angle value is relevant to the choice of materials and number of braiding yarns rather than the initial wrap angle. The data in Fig.18 were calculated according to the critical angle value of $\theta$=5.1° instead of $\theta$=0° (i.e. the stiff yarn was fully straightened) based on the experimental results obtained before. It can be found that a lower initial wrap angle gives a higher maximum NPR value and causes the ATB to be auxetic at an earlier level of strain. Clearly, the initial wrap angle is a quite influential design parameter in altering the auxeticity of the ATB structure.

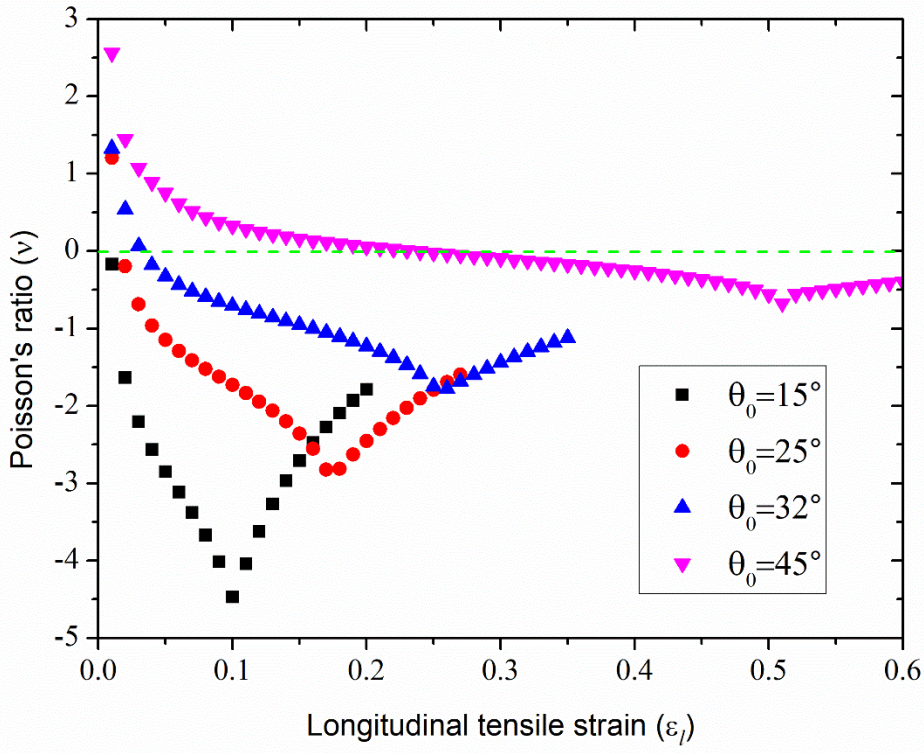


Fig. 18. Poisson's ratio vs. initial helical angle of stiff wrap yarn for the ATB structures made with the same materials.

## 5. Conclusions

A theoretical analysis on the deformation behaviour of the ATB structure was carried out in this study. The calculated results from the model developed were compared with the

experimental ones in order to valid its accuracy. Using developed model, the deformation behaviour and auxetic effect of ATB can be studied. According to the theoretical analysis, the following conclusions are drawn.

(1) The model developed in this study can correctly predict the variation trend of the auxetic behavior of the ATB structure, which first increases and then decreases with the increase of the axial strain. This prediction provides a better understanding of the deformation behavior of the ATB under axial extension.

(2) In real condition, the stiff yarn cannot be fully straightened before it breaks and its helical angle decreasing rate is inconsistent during the stretching.

(3) The difference in the Poisson's ratio values between the experiment and the theoretical calculations at large tensile strains mainly comes from the unrealistic assumption that the stiff wrap yarn can be fully straightened before it breaks. In order to get a better prediction, an adjustment based on the experiment is necessary for the stage of deformation at high tensile strains. On the other hand, a finite element analysis on Poisson's ratio behaviour of ATB under tension needs to be conducted in the future study because the mechanical reactions between yarn components cannot be taken into consideration in a pure geometry analytical analysis.

**Acknowledgement**

This work was supported by the Research Grants Council of Hong Kong Special Administrative Region Government (grant number 15203615) and The Hong Kong Polytechnic University in form of an internal project (grant number YBUZ).

## Reference


[1] K. E. Evans, M. A. Nkansah, I. J. Hutchinson, S. C. Rogers. Molecular network design. Nature, 1991. 353(6340): 124-124.

[2] W. Yang, Z. M. Li, W. Shi, B.H. Xie, M. B. Yang. Review on auxetic materials. Journal of materials science, 2004. 39(10): 3269-3279.

[3] F. Scarpa, F. C. Smith. Passive and MR fluid-coated auxetic PU foam–mechanical, acoustic, and electromagnetic properties. Journal of intelligent material systems and structures, 2004,15(12): 973-979.

[4] K. L. Alderson, A. Fitzgerald, and K. E. Evans. The strain dependent indentation resilience of auxetic microporous polyethylene. Journal of Materials Science, 2000. 35(16): 4039-4047.

[5] R. Lakes, K. Elms. Indentability of conventional and negative Poisson's ratio foams. Journal of Composite Materials, 1993,27(12): 1193-1202.

[6] K. W. Wojciechowski. Constant thermodynamic tension Monte-Carlo studies of elastic properties of a two-dimensional system of hard cyclic hexamers. Mol Phys 1987,61(5):1247-1258.

[7] K.W. Wojciechowski, A. C. Branka. Negative Poisson ratio in a two-dimensional ‘‘isotropic’’ solid. Phys Rev A 1989,40(12):7222-7225.

[8]R. Lakes. Foam Structures with a Negative Poisson's Ratio. Science, 1987, 235(4792): 1038-40.

[9] T. C. Lim. Auxetic materials and structures. Springer, Singapore, 2015.

[10] H.Hu, M Zhang, Y. Liu. Auxetic Textiles, Elsevier, 2019.

[11] K. L. Alderson, K. E. Evans. The fabrication of microporous polyethylene having a negative Poisson's ratio. Polymer, 1992. 33(20): 4435-4438.

[12] K. L. Alderson, A. Alderson, G. Smart, V. R. Simkins, P. J. Davies. Auxetic polypropylene fibres Part 1 - Manufacture and characterisation. Plastics Rubber and Composites, 2002. 31(8): 344-349.

[13] Y. Liu, H. Hu, J. K. C. Lam, S. Liu. Negative Poisson’s ratio weft-knitted fabrics. Textile Research Journal, 2010. 80(9): 856-863.

[14] K. Alderson, A. Alderson, S. Anand, V. Simkins, S. Nazare, N. Ravirala. Auxetic warp knit textile structures. Physica Status Solidi B-Basic Solid State Physics, 2012. 249(7): 1322-1329.

[15] T.C. Lim. Semi-auxetic yarns. physica status solidi (b), 2014. 251(2): 273-280.

[16] P. Subramani. S. Rana. D. V. Oliveir. R. Fangueiro. J. Xavier. Development of novel auxetic structures based on braided composites. Materials & Design, 2014. 61: 286-295.
[17] P. Hook. Auxetic mechanisms, structures & materials. 2003, Ph. D. thesis, School of Engineering and Computer Science, University of Exeter.
[18] A. Zulifqar, T. Hua, and H. Hu. Development of uni-stretch woven fabrics with zero and negative Poisson's ratio. Textile Research Journal, 2018, 88(18): 2076-2092.
[19] R. Caruana-Gauci , E. P. Degabriele, D. Attard, J. N. Grima. Auxetic metamaterials inspired from wine-racks. J Mater Sci, 2018, 53:5079-5091.
[20] M. Sloan, J. Wright, K. Evans. The helical auxetic yarn–a novel structure for composites and textiles; geometry, manufacture and mechanical properties. Mechanics of Materials, 2011,43(9): 476-486.
[21]G. H. Zhang, O. Ghita, C. Lin, K. E. Evans, Varying the performance of helical auxetic yarns by altering component properties and geometry. Composite Structures, 2016. 140: 369-377.
[22] J. McAfee, N.H. Faisal. Parametric sensitivity analysis to maximise auxetic effect of polymeric fibre based helical yarn. Composite Structures, 2017. 162: 1-12.
[23]S. Bhattacharya, G. H. Zhang, O. GhitaK, E.Evans. The variation in Poisson's ratio caused by interactions between core and wrap in helical composite auxetic yarns. Composites Science and Technology, 2014. 102: 87-93.
[24]J. R. Wright, M. R. Sloan, K.E. Evans. Tensile properties of helical auxetic structures: A numerical study. Journal of Applied Physics, 2010. 108(4): 044905.
[25] Z. Du, M. Zhou, H. Liu and L. He. Study on negative Poisson's ratio of auxetic yarn under tension: Part 1–Theoretical analysis. Textile Research Journal, 2015. 85(5): 487-498.
[26] Z. Du, M. Zhou, L. He, H. Liu. Study on negative Poisson's ratio of auxetic yarn under tension: Part 2–Experimental verification. Textile Research Journal, 2015. 85(7): 768-774.
[27]J. R. Wright, M. K. Burns, E. James, M. R. Sloan, K. E. Evans. On the design and characterisation of low-stiffness auxetic yarns and fabrics. Textile Research Journal, 2012. 82(7): 645-654.
[28]W. Miller, P. B. Hook, C. W. Smith, X.Wang, K. E. Evans. The manufacture and characterisation of a novel, low modulus, negative Poisson's ratio composite. Composites Science and Technology, 2009. 69(5): 651-655.
[29] N. Jiang, H. Hu. A study of tubular braided structure with negative Poisson's ratio behavior. Textile Research Journal, 2018. 88(24): 2810-2824.